Revista Mexicana de Astronomía y Astrofísica, **52**, 113–124 (2016)

TIDAL SHEAR AND THE V1309 SCO MERGER

Gloria Koenigsberger[1] and Edmundo Moreno[2]

Received November 9 2015; accepted January 29 2016

RESUMEN

Se muestra que la disipación de energía $\dot{E}_S$ debida a la interacción por fuerzas de marea puede haber sido la responsable de la disminución en el período orbital observado en el sistema binario V1309, sistema en donde posiblemente han coalescido sus dos componentes. $\dot{E}_S$ aparece cuando la velocidad de rotación de las capas externas de una estrella binaria se salen de sincronía con el movimiento orbital. Mostramos que bajo este efecto, una estrella de $1M_\odot$ con una compañera de $0.8M_\odot$ puede aumentar su radio de $1.50R_\odot$ a $1.85R_\odot$ en un tiempo de $\simeq 5$ años. Mientras tanto, el período orbital disminuye al mismo ritmo que el observado en V1309 Sco. La viscosidad cinemática ν que utilizamos se estima a partir de las perturbaciones máximas de la componente horizontal de la velocidad y del radio estelar. Es decir, ν es función de los parámetros estelares y orbitales del sistema.

ABSTRACT

We show that the observed decline in the orbital period of the merger candidate V1309 Sco could have been driven by tidal shear energy dissipation, $\dot{E}_S$. This mechanism becomes relevant once the expanding layers of an evolving star rotate asynchronously. For a $1M_\odot + 0.8M_\odot$ system with orbital period P=1.44 d, we find that $\dot{E}_S$ can power a growth in stellar radius from $1.50R_\odot$ to $1.85R_\odot$ in the primary over the course of $\simeq 5$ years, during which the rate of period change goes from $\simeq 1000$ yr to $\simeq 170$ yr, in agreement with the observations. The kinematical viscosity used for these calculations is estimated from the maximum tidal flow speed and from the extension of the the tidal bulge, and is thus a function of the stellar and orbital parameters.

Key Words: binaries: close — stars: eclipsing — stars: individual — stars: novae

1. INTRODUCTION

V1309 Sco underwent a nova-like outburst in 2008 (Nakano 2008). Its characteristics were similar to those of the eruptions in V838 Mon in 2002 (Munari et al. 2002), V4332 Sgr in 1994 (Martini et al. 1999) and several extragalactic objects (Mould et al. 1990; Kulkarni et al. 2007; Berger et al. 2009). Soker & Tylenda (2003) proposed that the energy source of these events could be the merger of two low-mass stars, an idea that is now strongly supported by the events leading up to the V1309 Sco eruption and its subsequent observations.

The pre-outburst state of V1309 Sco was observed fortuitously by the OGLE-III and OGLE-IV[3] projects starting in 2001. These data, analized by Tylenda et al. (2011), indicate the presence of an eclipsing binary whose orbital period rapidly decayed: during 2002–2004, $P/\dot{P} \simeq$1000 yr while during 2006–2007, $P/\dot{P} \simeq$170 yr. The infrared colors indicate T_{eff}=4500 K, suggesting the presence of a solar-type star in the system and the eclipse light curve suggests that the shape of one or both of the stars was tidally-distorted. This led Tylenda et al. to conclude that the progenitor was a $\simeq 1\ M_\odot$ star near the start of the red giant branch. The absence of periodic photometric variations after the nova event led to the conclusion that the two objects had merged. This conclusion has been further strengthened by recent observations that show the presence of outflowing molecular gas and dust surrounding the object (Kamiński et al. 2015).

[1]Instituto de Ciencias Físicas, Universidad Nacional Autónoma de México, Cuernavaca, Morelos, México.

[2]Instituto de Astronomía, Universidad Nacional Autónoma de México, México, D.F., México.

[3]Udalski 2003; http://ogle.astrouw.edu.pl

The orbital evolution immediately prior to the merger was modeled under the assumption of angular momentum loss through magnetized stellar winds during two-thirds of the system's lifetime, followed by Roche lobe overflow (Stepień 2011). This model implies that during the time of the OGLE observations, V1309 Sco was already a contact system with the stars filling their Roche lobes.

In this paper we explore an alternative scenario that does not require mass loss nor that the stars be already filling the Roche lobe during the early phase of the period decline. Instead, we make use of the fact that, as a star expands during post-main sequence evolutionary phases, the rotation rate of its outer region becomes sub-synchronous, leading to tidal shear energy dissipation. We thus explore the possibility that the observed orbital decay in V1309 Sco was a consequence of this mechanism. We find that the behavior of $P/\dot{P}$ over the timescale during which this quantity was measured can indeed be reproduced in a straightforward manner with the tidal shear energy dissipation scenario. The method and assumptions are described in § 2. The results are presented in § 3 and discussed in § 4.

2. TIDAL SHEAR ENERGY DISSIPATION

The only basic facts known about V1309 Sco prior to its outburst are: (a) T_{eff}=4500 K, suggesting the presence of a solar-type star in the system; (b) a periodic light curve with two eclipses during the observations of 2002–2006 and only one eclipse at the end of the 2007 observing season; (c) a distorted light curve indicating a tidally deformed stellar shape; and (d) a systematically decreasing trend in the period, with $P/\dot{P} \simeq$1000 years during 2002–2004 and 170 years during 2006–2007.

Taken together, these facts indicate that we witnessed the end stages of physical processes that initiated slowly and accelerated over time. Consider the process by which a binary star evolves when it leaves the main sequence (MS): In general, as the core contracts, the outer region expands and assuming conservation of specific angular momentum, the rotation angular velocity of these layers decreases. Hence, a star that had attained synchronous rotation during its MS lifetime now becomes sub-synchronous (in its outer region). If the rate of expansion is faster than the synchronization timescales, then the star remains sub-synchronous for the remainder of the expansion phase.

As soon as the star becomes sub-synchronous, tidal shear energy dissipation becomes active. The amplitude of tidal perturbations and the energy dissipation rate increase rapidly with increasing stellar radius and/or decreasing orbital separation. In an equilibrium state, the energy that is deposited in the stellar layers as heat is transported outward and eventually lost through radiation. However, if the rate of shear energy dissipation is too large, the star becomes bloated, an outcome that has been analyzed for a variety of objects, including white dwarfs (Dall'Osso & Rossi, 2014) and planets (Bodenheimer et al. 2001; Gu et al. 2004; Leconte et al. 2009).

The bloating contributes to keep the rotation sub-synchronous and the tidal forces not only remain active but become more intense with each radius increase. Hence, the outcome of this process is most likely a runaway phenomenon. This is the scenario that we explore for V1309 Sco in the following sections.

2.1. *Model and assumptions*

The simplest model to assume is one in which V1309 Sco consists of a 1 $M_\odot$ primary star (m_1) that has recently left the main sequence. The companion is chosen[4] to be of 0.8 $M_\odot$. As described above, the expansion of the primary's outer region has caused its rotation rate to become subsynchronous with respect to the orbital period, leading to tidal shear energy dissipation, $\dot{E}_S$. This quantity, when added to the the rate of change of the rotation energy, $\dot{K}$, and of the gravitational potential energy, $\dot{W}$, must be compensated by a the change in orbital energy:

$$-\dot{E}_{orb} = \dot{E}_S + \dot{K} + \dot{W}\,. \tag{1}$$

Using the expression for the orbital energy $E_{orb} = -Gm_1m_2/2a$ and assuming no mass loss we have:

$$\dot{E}_{orb} = \frac{Gm_1m_e}{2a^2}\dot{a}\,, \tag{2}$$

where a is the orbital major semi-axis and G the gravitational constant. With Kepler's relation, $a^3 = (G/4\pi^2)(m1 + m2)P^2$, we can then write

$$\frac{\dot{E}_{orb}}{E_{orb}} = -\frac{2}{3}\frac{\dot{P}}{P}\,. \tag{3}$$

[4](a)The two equal eclipses in the light curve indicate the presence of two stars of initially similar characteristics. (b) The assumption that the phenomenon is caused by a star evolving off the MS implies that one of the objects is more massive than the other. (c) Kochanek et al. (2014) find that the rates are dominated by MS+MS mergers.

Assuming that the three terms of the right of equation (1) are approximately equal to each other leads to $\dot{E}_S \simeq -\dot{E}_{orb}/3$, and

$$\frac{E_S}{E_{orb}} \simeq \frac{2}{9}\frac{\dot{P}}{P}\,; \tag{4}$$

and thus,

$$\frac{P}{\dot{P}} \simeq \frac{-Gm_1m_2}{9aE_S}\,. \tag{5}$$

We compute $\dot{E}_S$ in the surface layers of m_1 as they respond to the presence of m_2 using the TIDES code (Moreno & Koenigsberger 1999; Moreno et al. 2011). The assumption is made that the lower-mass companion m_2 has not yet reached the end of its main sequence lifetime and thus it remains synchronous throughout the process that we describe.

The TIDES code computes $\dot{E}_S$ by solving the equations of motion for a grid of volume elements that constitute a shell S at radius r which encloses the mass m_1. The main body of m_1 interior to S is assumed to behave as a rigid body and the tidal deformation is assumed to occur only in S. The equations of motion include the gravitational forces of m_1 and m_2, and Coriolis, centrifugal, gas pressure and viscosity forces on m_1. The stellar equator is assumed to lie in the orbital plane and m_2 is treated as a point source.

Values of $\dot{E}_S$ are obtained for a set of successively increasing stellar radii, as listed in Column 1 of Table 1 which, when substituted into equation (5) provide values of $P/\dot{P}$. Each radius is assumed to correspond to a different point in time. In this manner, the expansion of the star is taken into consideration. However, the actual rate of expansion is *a priori* not known. In order to estimate it, we use the rate of change of the gravitational potential energy, $\dot{W}$, due to the expansion of the shell S whose mass is Δm, and, assuming no mass loss,

$$\dot{W} = \frac{Gm_r\Delta m}{r^2}\frac{dr}{dt}\,, \tag{6}$$

where m_r is the mass interior to the radius r of S. Making use of the approximation $\dot{W} \simeq \dot{E}_S$ and taking $m_r \simeq m_1$, since the mass contained in S is negligible compared to the total mass below it, we can write

$$\dot{E}_S \simeq \frac{Gm_1\Delta m}{r^2}\frac{dr}{dt}\,. \tag{7}$$

TABLE 1

RESULTS: NOMINAL CASE

$R(t_i)$ $R_\odot$	ν cm^2 s^{-1}	h $R_\odot$	Δv_φ^{max} km s^{-1}	ϵ^* Note[a]	$10\times\nu_{est}$ cm^2 s^{-1}
0.99	5.10e+13	0.0006	0.20	2.2	8.22e+12
1.20	5.10e+13	0.0014	0.53	11.5	5.12e+13
1.35	1.64e+14	0.0023	0.87	97.5	1.40e+14
1.38	1.59e+14	0.0025	0.97	114.1	1.68e+14
1.40	1.81e+14	0.0026	1.02	147.8	1.85e+14
1.44	2.27e+14	0.0030	1.13	236.1	2.35e+14
1.46	2.49e+14	0.0031	1.18	292.8	2.55e+14
1.48	2.72e+14	0.0033	1.24	359.4	2.83e+14
1.50	3.06e+14	0.0035	1.29	454.2	3.13e+14
1.55	3.91e+14	0.0040	1.41	773.9	3.93e+14
1.58	4.48e+14	0.0043	1.49	1052.7	4.47e+14
1.60	4.93e+14	0.0046	1.55	1300.4	4.96e+14
1.64	6.24e+14	0.0052	1.68	2058.4	6.07e+14
1.68	7.37e+14	0.0059	1.83	3009.5	7.51e+14
1.72	9.64e+14	0.0068	2.00	4751.5	9.46e+14
1.75	1.08e+15	0.0075	2.13	6074.0	1.11e+15
1.85	1.47e+15	0.0090	2.52	12633.8	1.58e+15
1.95	2.55e+15	0.0104	2.82	29381.3	2.04e+15
2.15	3.23e+15	0.0203	3.44	65725.8	4.86e+15
2.25	5.05e+15	0.0255	3.67	105290.0	6.51e+15

[a] ϵ^* is in units of 10^{35} ρ ergs/(s $-$ g/cm^3), where ρ is the mass density.

Thus,

$$\begin{aligned} t_{if} = \int_{t_i}^{t_f} dt &\simeq \frac{Gm_1\Delta m}{<\dot{E}_S>}\int_{r_i}^{r_f}\frac{dr}{r^2} \\ &\simeq \frac{Gm_1\Delta m}{<\dot{E}_S>}\left(\frac{1}{r_i}-\frac{1}{r_f}\right), \end{aligned} \tag{8}$$

which gives the time it takes the shell S to expand from r_i to r_f, due to the energy input $<\dot{E}_S>$, the latter being the average of the computed $\dot{E}_S$ values at r_i and r_f. The time that has elapsed since an initial epoch t_0 is then

$$t \simeq t_0 + \sum_{if=1}^{n} t_{if}\,. \tag{9}$$

2.2. *Input parameters*

The input parameters for the $\dot{E}_S$ calculation are the stellar masses (m_1, m_2), the radius r_i of S, the synchronicity parameter ($\beta_0 = \omega/\Omega_0$), the orbital

period and eccentricity (P, e), the kinematical viscosity (ν), the equation of state, the thickness of S ($c_{\Delta R}\ r_i$), the grid size (N_φ, N_θ), the tolerance for the Runge-Kutta integration of the equations of motion (Tol), and the number of orbital cycles needed to reach the stationary state (N_{cycle}).

For V1309 Sco, we adopt $m_1 = 1\,M_\odot$, $m_2 = 0.8\,M_\odot$, P=1.44 d, e=0, $\beta_0 = 0.95$, $c_{\Delta R} = 0.02$. The equation of state is assumed to be polytropic, $p = p_0(\rho/\rho_0)^{\gamma'}$, with $\gamma' = 1 + 1/n$, n the polytropic index and ρ the mass density. For the present calculations we used $n = 1.5$, following the suggestion of Press et al. (1975) who note that the temperature gradient in asynchronous binaries ought to be nearly adiabatic rather than that given by radiative opacities, so that the turbulent envelope should be roughly an $n = 3/2$ polytrope.

All computations are performed with a grid size (N_φ, N_θ)=(500,20) which covers half a hemisphere from the equator to a co-latitude of 85°. The tolerance of the Runge-Kutta integration scheme was chosen Tol=10^{-11}–10^{-7}, depending on the particular case, and N_{cycle}=37.

The largest uncertainty in the input parameters involves the choice of ν, the kinematical viscosity. The standard molecular viscosity is $\simeq$1–10^5 cm^{2}s^{-1}, orders of magnitude smaller than the values typically used in models of astrophysical phenomena (Adame et al. 2011; Alexander 1973; Sutantyo 1974; Hansen 2010; Penev et al. 2007) or derived from observational data (Pérez de Tejada 1999). The general idea is that turbulence can enhance by many orders of magnitude the value of ν. Although progress is being made in understanding the turbulent viscosity (c.f., Penev et al. 2007; 2009 for stars; Ogilvie & Lesur 2012 for protoplanetary disks), the actual value for the viscosity to be used in particular problems is still unconstrained.

A standard expression for the turbulent viscosity involves the definition of a *length scale*, h, associated with the size of the turbulent eddies, and a *velocity scale*, v_{turb}, which is the typical velocity of these eddies. For accretion disks, a simple parametrization of these two scales was proposed by Shakura & Sunyaev (1973). For the length scale, they assumed isotropy and characterized it by the typical size of the largest turbulent eddies, which cannot exceed the local pressure scale height, H. For the velocity scale they reasoned that if the turbulent velocity were supersonic, the associated shock waves would have the effect of dissipating energy and thus reducing the velocity to the sound speed, c_s, or smaller. Hence, $v_{turb} \leq c_s$. From these considerations, they arrived at the α-prescription for the viscosity: $\nu \simeq \alpha H c_s$, where α takes on values 0–1.

Guided by these ideas, we explored the use of the following prescription for estimating ν:

$$\nu_{est} \simeq \alpha_T\ h\ \Delta \mathrm{v}_\varphi^{max}\,, \tag{10}$$

where h is the height of the major bulge in the equilibrium tide approximation and $\Delta \mathrm{v}_\varphi^{max}$ is the maximum azimuthal velocity perturbation. α_T is a parameter that takes into account factors that are additional to the tidal perturbation, such as magnetic fields and convection, as well as the timescale for the propagation of perturbations. Considering that the latter is the sound speed, c_s, an analogy with the Shakura & Sunyaev (1973) prescription provides a rough estimate $\alpha_T \Delta \mathrm{v}_\varphi^{max} \simeq c_s$. Since $\Delta \mathrm{v}_\varphi^{max} << c_s$, we expect $\alpha_T >> 1$.

2.3. *Method of computation*

A set of stars with radii r_i in the range 0.99 – 2.25 $R_\odot$ was chosen for computation with `TIDES`, using a shell thickness $c_{\Delta R} r_i = 0.02 r_i$.

The computations were conducted in two steps. In the first step, ν was chosen close to the smallest value that allows `TIDES` to arrive at a stationary solution.[5] This computation provided a first set of values of h and $\Delta \mathrm{v}_\varphi^{max}$. Considering that $c_s \simeq 20 - 30$ km s^{-1} (Guenther et al. 1992; for a shell located at $0.98 R_\odot$ in a standard solar model) and that $\Delta \mathrm{v}_\varphi^{max} \simeq 2 - 3$ km s^{-1} (see below), we adopted α_T=10 for $r_i > 1\ R_\odot$. This yielded the values of ν (Column 2 of Table 1) that were used in the second step.

The values of h and $\Delta \mathrm{v}_\varphi^{max}$ obtained in the second step calculation are listed in Columns 3 and 4 of Table 1, and Column 6 lists the corresponding values of ν_{est}. The differences between these new values and the ones obtained in the previous step are minor. This is because h and $\Delta \mathrm{v}_\varphi^{max}$ do not depend strongly on the chosen value of viscosity.

The output of the `TIDES` calculation is the quantity

$$\epsilon^* = \dot{E}_S / 10^{35} \rho, \tag{11}$$

[5] When the tidal forcing is too strong compared to the restoring forces, the perturbation amplitudes systematically increase causing the surface elements to become detached from the grid, or the center of mass of neighboring elements to interchange positions, both of which cause the computation to halt.

where $\dot{E}_S/10^{35}$ is the energy dissipation rate in units of 10^{35} ergs s^{-1} and ρ is the average mass density in shell S in units of g cm^{-3}. The values of ϵ^* that were obtained are listed in Column 5 of Table 1.

Equations (6) and (9) require Δm, the mass contained in S, and its average density, ρ, for which a stellar structure model is required. As will be seen below, the timescale over which tidal shear energy dissipation can cause a layer to expand is very short compared to evolutionary timescales. Stellar evolution models for low-mass stars do not contemplate such short timescales because changes in a single star occur over much longer times. For example, it takes the radius of a post-main sequence 1 $M_\odot$ star 16.6 Myr to increase from 2.50 to 2.55 $R_\odot$. Furthermore, it is not even clear whether a stellar structure model for a single star is a valid approximation for a tidally perturbed star. Hence, in what follows, we first adopt the hypothesis that the outer layers of an asynchronous binary star can be approximated with a n=1.5 polytropic structure (Press et al. 1975), which provides ρ and Δm. In the second approach, no assumption is made concerning the manner in which the outer layers expand, thus allowing for an arbitrary density structure. $\dot{E}_S$ is obtained by adjusting the parameter $N\Delta m$, which is the total mass involved in the energy dissipation and expansion processes.

2.4. *Polytropic structure*

The stellar structure of 1 $M_\odot$ n=1.5 polytrope was computed for stars of radii R_{poly}=1–2.3 $R_\odot$. These models provide ρ_0, the central density and $(\rho/\rho_0)_{shell}$, the relative density, as a function of shell radius, R_{shell}. The nature of polytropes is such that, given a stellar mass, ρ/ρ_0 is constant for a fixed value of R_{shell}/R_{poly}, for all R_{poly}. Furthermore, $\rho_0 = \rho_1(R_{poly1}/R_{poly})^3$, where ρ_1 is a reference central density, here chosen to be that of the $R_{poly1} = 1\,R_\odot$ model, ρ_1=8.453 g/cm^3. Hence, for each shell radius, the density is

$$\rho/(g/cm^3) = \rho_1 \frac{(\rho/\rho_0)_{shell}}{(R_{poly}/R_{poly1})^3}\,. \qquad (12)$$

We list in Table 2 the value of $(\rho/\rho_0)_{shell}$ for the base of shells located at R_{shell}/R_{poly}=0.94, 0.96, 0.97, 0.975 and 0.98. Also listed in this table is Δm, which is constant for a shell located at a fixed R_{shell}/R_{poly}, of thickness $c_{\Delta R}R_{poly}$ for all R_{poly}, with a constant $c_{\Delta R}$.

TABLE 2

PROPERTIES OF POLYTROPIC SHELLS

(R_{shell}/R_{poly})[a]	(ρ/ρ_0)[b]	Δm[c] $M_\odot$
0.94	0.01017	0.00246
0.95	0.00771	0.00182
0.96	0.00540	0.00118
0.97	0.00344	0.00065
0.98	0.00184	0.00025

[a]The depth listed corresponds to the base of the shell.

[b]Density at the base of the shell in units of the central density.

[c]Mass contained in the shell.

2.5. *Arbitrary density variation in expanding layers*

It is possible to circumvent the use of ρ and Δm required by equations (5) and (9) by defining a layer L that is larger than the shell S that we model, and by assuming that the mass contained within L remains constant as the star (and the layer) expands. We assume that there is a number of such layers, N, and that the mass involved in both the tidal shear energy dissipation process and in the expansion process is $N\Delta m$. In the Appendix we provide the details of the mathematical manipulations that allow us to write $P/\dot{P}$ in terms of $N\Delta m$ and which yield t which is independent of the unknown ρ and Δm values.

3. RESULTS

3.1. *Polytropic structure*

We explored the behavior of polytropic shells at various depths by comparing the trend of $P/\dot{P}$ *vs.* t from equations (5) and (9) with that which is derived from a fit to the observations. Specifically, Tylenda et al. (2011) find that the observed variations of P over the time span 2002 to 2007 are given by $P/\mathrm{d} = 1.4456\,\exp[15.29/(t-t_0)]$, with $t_0 = JD = 2455233.5$ and $t < t_0$. Thus,

$$-P/\dot{P} = \frac{(t-t_0)^2}{15.29}\,. \qquad (13)$$

The uncertainty $\delta(P/\dot{P})$ in this relation can be derived by propagating the uncertainties given for P and t on Tylenda et al.'s Figure 2. We find that at JD = 24452870 and JD = 24454250, $\delta(P/\dot{P})$ ≃51 and 5 yr, respectively. The uncertainty δt ≃50 and ≃10 d is the same as given in this figure. The above-stated times correspond to $P/\dot{P}$=1000 and 170 yr,

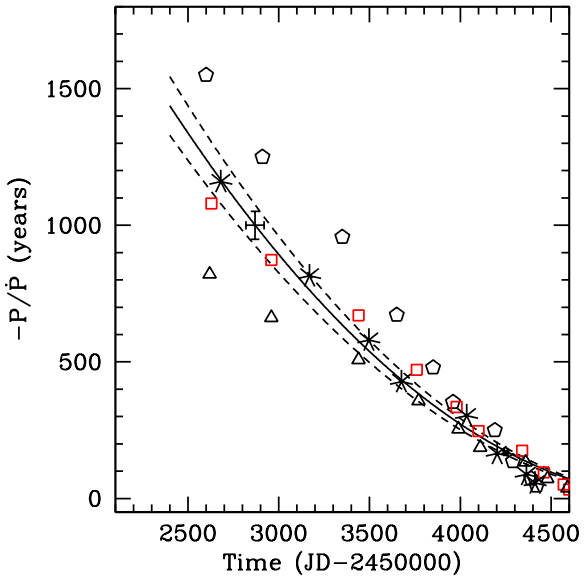

Fig. 1. Trend of $P/\dot{P}$ over time t for 1 $M_\odot$ polytropic stars of radii R_{poly}, for shells located at $0.94R_{poly}$ (triangles), $0.95R_{poly}$ (squares) and $0.96R_{poly}$ (pentagons). Also shown is the result for the approximation described in the Appendix, with $N\Delta m$=0.0016 $M_\odot$ (stars). The solid curve corresponds to the observational constraints (equation 13). The error bars located at $JD = 24452870$ and $JD = 24454250$ correspond to the propagated uncertainty from the error bars in Figure 2 of Tylenda et al. (2011). The dashed curves are indicative of the uncertainty over the range of dates shown in the figure. Model data were shifted along the time axis so as to coincide with the curve around $JD = 2454250$, where the propagated uncertainties on the observations are smallest.

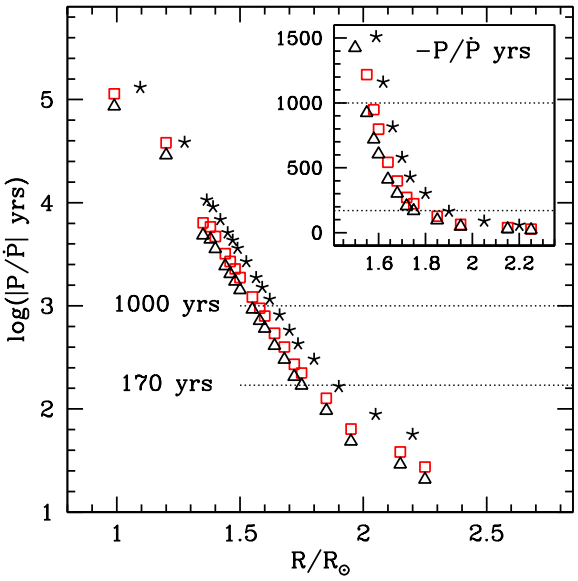

Fig. 2. $P/\dot{P}$ for 1 $M_\odot$ polytropic stars for shells located at $0.94R_{poly}$ (triangles) and $0.95R_{poly}$ (squares). Also shown is the $N\Delta m$ approximation (stars) described in the Appendix. The dotted lines enclose the region corresponding to the observations reported in Tylenda et al. (2011), providing the range in R_{poly} values that correspond to the dates of observation. The inset shows the same data on a linear scale for $P/\dot{P}$ <1600 yr.

respectively. The curve from equation (13) and the associated uncertainty (dashed line) are plotted in Figure 1 and compared to the results derived from the tidal energy dissipation calculations.

The best agreement is obtained with a polytropic shell whose base lies at 0.95 R_{poly}. Shells that are deeper or more superficial diverge significantly from the observational curve. As listed in Table 1, this shell contains Δm=0.0018 $M_\odot$. During the timeframe in which the orbital period was observed to decay, our results indicate that the stellar radius increased from ≃1.6 $R_\odot$ to 1.8 $R_\odot$, as illustrated in Figure 2.

Table 3 lists the values of the physical quantites that were computed using the polytropic stellar structure approximation for R_{shell}/R_{poly}=0.95. Columns 1 and 2 contain, respectively, the radii at t_i and t_f; Columns 3 and 4 contain $\dot{E}_S$ for the respective radii; Columns 5 and 6 contain the corresponding $P/\dot{P}$; Column 7 lists the time required for the shell to expand from $R(t_i)$ to $R(t_f)$; and Column 8 lists t, the time that has elapsed since the star first became asynchronous. We will refer to this case as the *nominal case*.

3.2. *Arbitrary density variation in expanding layers*

Equations (18), (22) and (9) were used with the data of Table 1 to obtain the trend in $P/\dot{P}$ *vs.* t for a broad range in $N\Delta m$ values. The best match to the observations was attained with $N\Delta m$=0.0016 $M_\odot$, a value remarkably similar to that obtained in the *nominal case* described above. These results are also plotted in Figure 1 and listed in Table 4. During the epoch for which observations are reported, the stellar radius is found to have increased from ≃1.60 $R_\odot$ to 1.85 $R_\odot$, which is also consistent with the result of the *nominal case*.

3.3. *Dependence on m_2, ν and polytropic index*

Additional calculations were performed to explore the dependence on m_2, ν and polytropic index, n. Each of these input parameters was changed, one by one, keeping the others fixed.

TABLE 3

PHYSICAL QUANTITIES 1: POLYTROPE, SHELL 0.95[a]

$R(t_i)$ $R_\odot$	$R(t_f)$ $R_\odot$	$\dot{E}_{Si}$ ergs s^{-1}	$\dot{E}_{Sf}$ ergs s^{-1}	$(-P/\dot{P})_i$ ergs s^{-1}	$(-P/\dot{P})_f$ years	t_{if} years	t years
0.990	1.200	1.45e+34	4.34e+34	1.14e+05	3.80e+04	1336.39	1336.
1.200	1.350	4.34e+34	2.58e+35	3.80e+04	6.39e+03	134.32	1471.
1.350	1.380	2.58e+35	2.83e+35	6.39e+03	5.83e+03	13.02	1484.
1.380	1.400	2.83e+35	3.51e+35	5.83e+03	4.70e+03	7.15	1491.
1.400	1.440	3.51e+35	5.15e+35	4.70e+03	3.20e+03	10.02	1501.
1.440	1.460	5.15e+35	6.13e+35	3.20e+03	2.69e+03	3.69	1505.
1.460	1.480	6.13e+35	7.23e+35	2.69e+03	2.28e+03	3.03	1508.
1.480	1.500	7.23e+35	8.77e+35	2.28e+03	1.88e+03	2.46	1510.
1.500	1.550	8.77e+35	1.35e+36	1.88e+03	1.22e+03	4.22	1514.
1.550	1.580	1.35e+36	1.74e+36	1.22e+03	9.49e+02	1.73	1516.
1.580	1.600	1.74e+36	2.07e+36	9.49e+02	7.97e+02	0.91	1517.
1.600	1.640	2.07e+36	3.04e+36	7.97e+02	5.42e+02	1.31	1518.
1.640	1.680	3.04e+36	4.14e+36	5.42e+02	3.99e+02	0.89	1519.
1.680	1.720	4.14e+36	6.09e+36	3.99e+02	2.71e+02	0.59	1520.
1.720	1.750	6.09e+36	7.39e+36	2.71e+02	2.23e+02	0.32	1520.
1.750	1.850	7.39e+36	1.30e+37	2.23e+02	1.27e+02	0.66	1521.
1.850	1.950	1.30e+37	2.58e+37	1.27e+02	6.39e+01	0.31	1521.
1.950	2.150	2.58e+37	4.31e+37	6.39e+01	3.83e+01	0.30	1521.
2.150	2.250	4.31e+37	6.02e+37	3.83e+01	2.74e+01	0.09	1521.

[a]The shell has a thickness of 0.02 R_{poly}; its base lies at $0.95R_{poly}$.

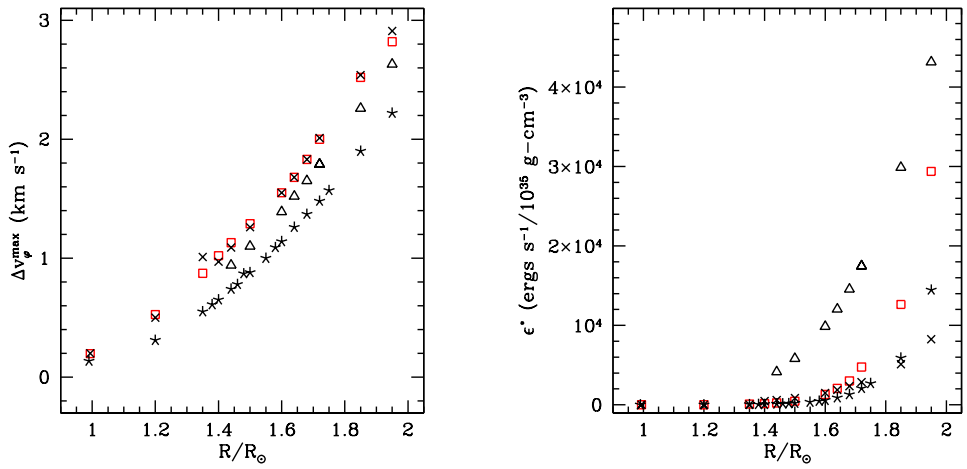

Fig. 3. Dependence of the azimuthal velocity, Δv_φ (left) and energy dissipation rate per unit density (right), as a function of radius and value of m_2 and ν. *Square:* $10\times\nu_{est}$, as in Figures 1 and 2; *Cross:* ν_{min}, approximately the smallest value for which the code runs for that particular radius; *Triangle:* $\nu \simeq 9\times\nu_{min}$; *Star:* m_2=0.4 $M_\odot$.

TABLE 4

PHYSICAL QUANTITIES 2: ARBITRARY EXPANSION STRUCTURE, $N\Delta M$=0.0016 $M_\odot$

$R(t_i)$ $R_\odot$	$R(t_f)$ $R_\odot$	$<\epsilon*>$[a]	$<E_S>$ ergs s^{-1}	$<-P/\dot{P}_{if}>$ years	t_{if} years	t years
0.99	1.20	6.8	1.67e+34	1.31e+05	1718.37	1718.
1.20	1.35	54.5	8.70e+34	3.85e+04	179.11	1897.
1.35	1.38	105.8	1.56e+35	1.06e+04	19.75	1917.
1.38	1.40	130.9	1.83e+35	9.12e+03	10.84	1928.
1.40	1.44	191.9	2.50e+35	6.84e+03	15.10	1943.
1.44	1.46	264.5	3.26e+35	5.10e+03	5.60	1949.
1.46	1.48	326.1	3.85e+35	4.31e+03	4.60	1953.
1.48	1.50	406.8	4.61e+35	3.61e+03	3.74	1957.
1.50	1.55	614.0	6.44e+35	2.68e+03	6.34	1963.
1.55	1.58	913.3	8.92e+35	1.88e+03	2.62	1966.
1.58	1.60	1176.6	1.10e+36	1.51e+03	1.38	1967.
1.60	1.64	1679.4	1.47e+36	1.16e+03	1.97	1969.
1.64	1.68	2533.9	2.07e+36	8.15e+02	1.34	1971.
1.68	1.72	3880.5	2.95e+36	5.80e+02	0.89	1972.
1.72	1.75	5412.8	3.89e+36	4.28e+02	0.49	1972.
1.75	1.85	9353.9	5.88e+36	3.03e+02	0.98	1973.
1.85	1.95	21007.6	1.12e+37	1.65e+02	0.46	1974.
1.95	2.15	47553.6	1.99e+37	8.85e+01	0.44	1974.
2.15	2.25	85507.9	2.98e+37	5.69e+01	0.13	1974.

[a] ϵ^* is in units of 10^{35} ρ ergs/(s $-$ g/cm^3), where ρ is the mass density.

The results obtained from the grid of calculations for $n = 3$ yielded values of ϵ^* that differed from those of the *nominal case* by <4 % for R <2$R_\odot$. For the cases run with R >2$R_\odot$ the differences increased up to 13%, with the $n = 3$ cases resulting in larger values of ϵ^*; this, however does not significantly modify the results obtained with the *nominal case*.

The results obtained from a grid of calculations with m_2=0.4 $M_\odot$ show that the energy dissipation rate decreases by a factor of ≃2 for R <2 $R_\odot$, i.e., proportional to the decrease of m_2. As a consequence, for a given radius of m_1, the azimuthal velocity perturbations and the energy dissipation rates are significantly smaller than those of the *nominal case*, as shown in Figure 3.

Computations were performed using a range of ν values, starting with the smallest value that allows the code to run. The results of these computations are listed in Table 5 and show that for R <1.7 $R_\odot$, ϵ^* is directly proportional to the value of ν. For larger radii an increase in ν leads to a smaller increase in the value of ϵ^*. This is because very large viscosities reduce the amplitude of horizontal motions which, in turn, lead to smaller energy dissipation rates.

Using the approximate linear proportionality for R <1.7 $R_\odot$, we scaled the ϵ^* obtained in the nominal calculation by factors of 0.1 and 5, to obtain approximate results for viscosities ν=ν_{est} and ν=50ν_{est}, respectively.[6] The derived trend in $P/\dot{P}$ *vs.* t in the polytropic approximation is plotted in Figure 4, which shows that the viscosity used in the nominal case does indeed provide the best coincidence with the observations.

The results of these tests are summarized in Table 6. Case 1 is the *nominal case*, which comes closest to reproducing the observations, and yields $P/\dot{P}$ values that go from −1000 yr to −170 yr over a ≃5 year timescale. Case 3 has a viscosity larger by a factor of 5 and the timeframe for the period decay for R >1.40 is consistent with the observations, but there is a significant discrepancy for smaller radii.

[6] The nominal case is computed with ν=10ν_{est}.

TABLE 5

VISCOSITY DEPENDENCE

$R(t_i)$ $R_\odot$	ν cm^2 s^{-1}	h $R_\odot$	Δv_φ^{max} km s^{-1}	ϵ^{*a}	ν_{est} cm^2 s^{-1}
0.99	5.04e+13	0.0006	0.20	2.2	8.22e+11
0.99	5.60e+13	0.0006	0.20	2.4	8.35e+11
1.20	5.04e+13	0.0014	0.53	11.5	5.12e+12
1.20	1.12e+14	0.0014	0.50	24.6	4.87e+12
1.35	5.60e+13	0.0023	1.01	36.8	1.62e+13
1.35	1.62e+14	0.0023	0.87	97.5	1.40e+13
1.40	1.79e+14	0.0026	1.02	147.8	1.85e+13
1.40	5.60e+14	0.0027	0.97	459.9	1.82e+13
1.44	2.24e+14	0.0030	1.13	236.1	2.36e+13
1.44	5.60e+14	0.0030	1.09	588.5	2.27e+13
1.44	5.04e+15	0.0027	0.94	4150.0	1.77e+13
1.50	3.02e+14	0.0035	1.29	454.2	3.14e+13
1.50	5.60e+14	0.0035	1.26	840.8	3.07e+13
1.50	5.04e+15	0.0032	1.10	5812.0	2.45e+13
1.60	4.87e+14	0.0046	1.55	1300.4	4.96e+13
1.60	5.60e+14	0.0046	1.55	1493.2	4.96e+13
1.60	5.04e+15	0.0041	1.39	9859.0	3.96e+13
1.64	5.60e+14	0.0052	1.68	1875.8	6.08e+13
1.64	6.16e+14	0.0052	1.68	2058.4	6.08e+13
1.64	5.04e+15	0.0046	1.52	12027.0	4.86e+13
1.68	5.60e+14	0.0059	1.83	2340.5	7.51e+13
1.68	7.28e+14	0.0059	1.83	3009.5	7.51e+13
1.68	5.04e+15	0.0051	1.65	14557.0	5.85e+13
1.72	5.60e+14	0.0068	2.01	2862.8	9.51e+13
1.72	9.52e+14	0.0068	2.00	4751.5	9.46e+13
1.72	5.04e+15	0.0057	1.79	17473.0	7.10e+13
1.72	5.04e+15	0.0057	1.79	17473.0	7.10e+13
1.85	5.60e+14	0.0084	2.54	5113.0	1.48e+14
1.85	1.46e+15	0.0090	2.52	12633.8	1.58e+14
1.85	5.04e+15	0.0087	2.26	29871.2	1.37e+14
1.95	5.60e+14	0.0125	2.91	8257.8	2.53e+14
1.95	2.52e+15	0.0104	2.82	29381.3	2.04e+14
1.95	5.04e+15	0.0117	2.63	43157.4	2.14e+14

*Results obtained from computations using different values of ν while holding all other input parameters constant.

[a]ϵ^* is in units of 10^{35} ρ ergs/(s − g/cm^3), where ρ is the mass density.

Case 2 has a viscosity smaller by a factor of 10 with respect to the nominal case, and the time required for $P/\dot{P}$ to cover the observed range is > 7 yr, significantly longer than in the other two cases. Case 4, which was run with m_2=0.4 $M_\odot$ and the viscosity of the *nominal case* also has significantly longer timescales than observed. This does not, however, eliminate the possibility of a smaller m_2, but a grid of models for $m_2 \simeq 0.4$ (and other values) needs to be constructed using a range of values of ν in order to estimate constraints for the secondary mass.

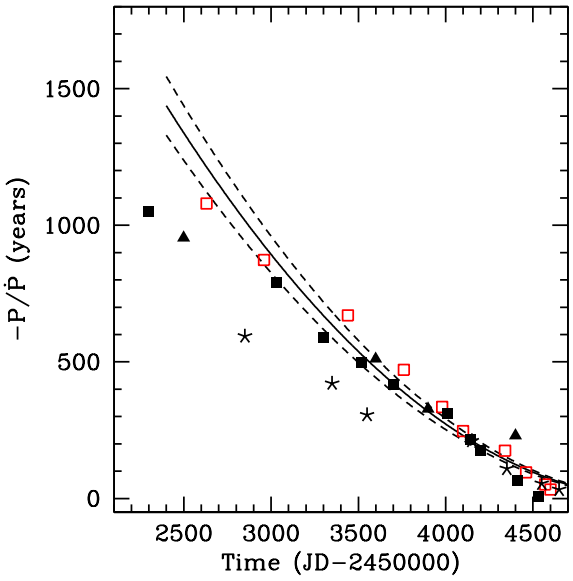

Fig. 4. Comparison of results from runs with values of ν and m_2 different from the nominal case (open squares). The curves are the same as shown in Figure 2. The other symbols correspond to: $\nu = 50\nu_{est}$ (filled rectangles), $\nu = \nu_{est}$ (triangles), and $m_2 = 0.4\ M_\odot$ (stars).

4. DISCUSSION

We propose that the orbital period decline observed in V1309 Sco was powered by tidal shear energy dissipation, $\dot{E}_S$. This mechanism first becomes active when the radius of the initially synchronously rotating star increases as it leaves the main sequence causing outer stellar layers to become subsynchronous. Initially, $\dot{E}_S$ is very small and $P/\dot{P}$ is very large, but as the radius increases, the rate of period decline accelerates. The heat deposited in the stellar layers due to $\dot{E}_S$ contributes to the rate of increase of the radius, thus eventually producing a runaway process where each radius increase results in an increase in $\dot{E}_S$ which, in turn, powers an additional radius increase.

V1309 Sco is assumed to consist of a 1+0.8 $M_\odot$ binary, the more massive component having left the main sequence and having a subsynchronous rotation rate. Our calculations of $\dot{E}_S$ produce the same trend in $P/\dot{P}$ as that observed over the 2002–2007 timeframe and indicate that the radius increased from

TABLE 6

DEPENDENCE ON ν AND M_2

Case	$R(t_i)$ $R_\odot$	$R(t_f)$ $R_\odot$	$< -P/\dot{P}_{if} >$ years	t years	Comment
1	1.55	1.58	1080	1516.0	nominal case
	1.75	1.85	175	1520.7	$\nu = 10 \times \nu_{est}$
2	1.85	1.95	954	15208.5	"smaller" ν
	2.25	2.50	230	15215.6	$\nu = \nu_{est}$
3	1.38	1.40	1050	298.2	"larger" ν
	1.60	1.64	175	303.4	$\nu = 50 \times \nu_{est}$
4	1.58	1.60	1090	3770.0	m_2=0.4$M_\odot$
	1.75	1.85	211	3778.8	

Cases: 1 is the nominal case (i.e., computed with $\nu = 10\nu_{est}$); Cases 2 and 3 are obtained by assuming that $\dot{E}_S$ is directly proportional to ν and using data from Table 1; Case 4 is computed with the nominal input parameters except for $m_2 = 0.4M_\odot$.

$\simeq$1.55 to 1.8 $R_\odot$ during the 5 years in which eclipses were evident. The subsequent evolution would have involved an ever more rapid radius increase until Roche lobe dimensions were attained. Note that such rapid radius growth is impossible from evolutionary considerations. For example, grids given by Marques et al. (2008)[7] show that the time it takes the radius of a 1 $M_\odot$ star in its latest post-main sequence phases to increase from 2.50 to 2.55 $R_\odot$ is 16.6 Myr.

It is interesting to note that, within the assumptions of the processes and the approximations in the calculation, the mass involved in producing the observed $P/\dot{P}$ rate is only $\simeq$0.0016 $M_\odot$, i.e., approximately 10% of the mass in the outer convective region. One may speculate that this amount of mass should increase as the orbital separation shrinks beyond that which we have computed, thus accelerating the process by which the Roche lobe dimensions are attained.

The method we employ for the computation of the tidal shear energy dissipation, $\dot{E}_S$, is limited primarily by the fact that it neglects the presence of shells above the one being modeled, and that it neglects the perturbations of the layers below it. The absence of a shearing layer above implies that $\dot{E}_S$ is underestimated, particularly since the amplitude of perturbations increases with increasing stellar radius. This, however, may be partly compensated by the overestimate of $\dot{E}_S$ produced by the assumption of a rigidly rotating region below.[8] A multi-layer calculation would extend the energy dissipation and heating of the stellar material to deeper regions of the star and thus involve a larger fraction of the convective zone in the dissipation/expansion process. The ideal solution is a full 3D computation of the tidal perturbations combined with the evolution of orbital parameters and stellar rotation, which however, is currently not tractable.

It is also interesting to note that the timescale from the start of subsynchronous rotation to the phase of runaway radius increase leading up to the Roche lobe overflow dimensions is extremely short, a few thousand years. This suggests that objects such as V1309 Sco might be relatively common, as recently concluded by Kochenek et al. (2014), although the probability of observing them during this phase is likely to be very small due to its short duration. Clearly, the actual rates will depend on the distribution of orbital separation, on the component masses and, not least, on the opacity and viscosity of the surface layers. For example, we estimate

[7] http://www.astro.up.pt/corot/models/cesam/A/

[8] In a multi-layer calculation, the velocity gradients due to the perturbations are expected to be smaller than those occuring when only one layer is allowed to respond to the external perturbation.

that if ν is a factor of 10 smaller than that used in the *nominal case*, the timescale between the start of asynchronous rotation and the observed orbital period decay becomes a factor of $\simeq$10 larger.

We find a convenient scaling for the viscosity $\nu = \alpha_T\ h\ \Delta \mathrm{v}_\varphi^{max}$, where h is the height of the major bulge in the equilibrium tide approximation, $\Delta \mathrm{v}_\varphi^{max}$ is the maximum azimuthal speed of the tidal flow and α_T is a parameter that takes into account factors other than the tidal perturbations, such as magnetic fields and convection. Accordingly, since h and $\Delta \mathrm{v}_\varphi^{max}$ depend on the stellar and orbital parameters, the value of ν also depends on these quantities, an idea first suggested by Press et al. (1975). To achieve the agreement between our calculations and the observational constraint shown in Figure 1, we used α_T=10, resulting in $\nu = \nu(r) = 10^{13} - 10^{15}$ cm^2/s, with the larger values corresponding to larger radii.

The nature of tidal perturbations is such that their amplitude is largest in the equatorial plane, declining towards the polar ragions.[9] Hence, an interesting problem concerns the manner in which the energy that is deposited near the equatorial region due to tidal shear may affect the stellar structure. Relevant to the V1309 Sco event is the question of whether the increasing tidal shear energy dissipation rates have an impact on mass loss. Dynamical models (e.g., D'Souza et al. 2006) predict significant mass-loss associated with a merger. However, there might have been circumstellar matter present in the V1309 Sco system well before the outburst (McCollum et al. 2014). One may speculate that, in addition to triggering the initial orbital period decay, the tidal instabilities may provide sufficient energy for mass loss along the equatorial plane, well before the merger occurs.

We thank Frédéric Masset for a critical reading of the manuscript and very helpful suggestions, and we thank Matthew Bate and Norbert Langer for enlightening discussions. Computing support from Ulises Amaya, Alfredo Díaz, and Francisco Ruiz and financial support from UNAM/DGAPA/PAPIIT Project IN 105313 and CONACYT Project 129343 are gratefully acknowledged.

APPENDIX A. ARBITRARY DENSITY VARIATION IN EXPANDIG LAYERS

We assume that the outer region of the star is divided into N layers and we choose a layer, L, whose energy dissipation rate, $\dot{E}_L$, can be considered to be representative of this region. The layer has a mass Δm and at some initial time t_i, its thickness is Δ_i. Its mid-point lies at an equilibrium radius r_i. We impose the condition that the mass of the layer, Δm, remains constant. Hence, after a time t_{if}, when L has expanded to a new equilibrium radius r_f with a new thickness Δ_f, its mass remains the same.

We now choose a shell S within L, also centered on r_i, and whose thickness is Δ_i^*. The tidal shear energy dissipation rate in L and in S are, respectively, $\dot{E}_L = 10^{35} < \rho_i > \epsilon_i$ and $\dot{E}_S = 10^{35}\rho_i\epsilon_i^*$, where $< \rho >_i$ is the average density in the layer, and ϵ_i is its energy dissipation rate per unit density. The `TIDES` computation yields ϵ_i^*, and we assume that

$$\epsilon_i \simeq \epsilon_i^* \frac{\Delta_i}{\Delta_i^*}\,. \tag{A.1}$$

Thus the energy dissipation rate for the N-layers in the outer region is,

$$\dot{E}_{NL} \simeq N\dot{E}_L = N\dot{E}_S \frac{\Delta_i}{\Delta_i^*} = N10^{35}\rho_i\epsilon_i^* \frac{\Delta_i}{\Delta_i^*}\,. \tag{A.2}$$

The mass, radius, thickness and density of a spherical shell are related by

$$\rho_i\Delta_i = \frac{\Delta m}{4\pi r_i^2}\,. \tag{A.3}$$

Hence, we can write,

$$\dot{E}_{NL} \simeq \frac{10^{35}N\Delta m}{4\pi c_{\Delta R}} \frac{\epsilon_i^*}{r_i^3}\,. \tag{A.4}$$

Substituting the above in equation (5), but using $\dot{E}_{NL}$ instead of $\dot{E}_S$

$$\frac{P}{\dot{P}} \simeq \frac{-4\pi G m_1 m_2 r_i^3}{9\times 10^{35} a N \Delta m} \frac{c_{\Delta R}}{\epsilon_i^*}\,, \tag{A.5}$$

where we have used $\Delta_i^* = c_{\Delta R} r_i$.

For the time calculation we procede as in § 2.1, but now re-state equation (1) as

$$-\dot{E}_{orb} = \dot{E}_{NL} + \dot{K} + \dot{W}\,, \tag{A.6}$$

and $\dot{E}_{NL} \simeq \dot{W}$.

The change in gravitational potential energy of a surface layer of mass Δm at radius r_i with interior mass m_r is given by

$$\dot{W}_L = \frac{G m_r \Delta m}{r_i^2} \frac{dr}{dt}\,. \tag{A.7}$$

Because L is chosen to have a tidal shear energy dissipation rate that is representative of the entire region, we write

[9] Our model is curently designed only for cases in which the stellar rotation axis is parallel to the axis of orbital motion.

$$\dot{W} \simeq N\dot{W}_L \simeq \dot{E}_{NL}\,. \tag{A.8}$$

Combining equations (A.6), (A.7) and (A.8), and considering that the mass interior to the convective zone of a solar-type star is $\simeq$0.98 $M_\odot$ (c.f. Guenther et al. 1992) and that the region most strongly affected by the tidal shear is likely to lie very close to the stellar surface, so we can approximate $m_r \simeq m_1$,

$$\begin{aligned} \int_{t_i}^{t_f} dt &\simeq \frac{4\pi G c_{\Delta R} m_1}{10^{35} < \epsilon^*_{i,f} >} \int_{r_i}^{r_f} r_i dr \\ t_{if} = t_f - t_i &\simeq \frac{2\pi G c_{\Delta R} m_1}{10^{35} < \epsilon^*_{i,f} >} (r_f^2 - r_i^2) \end{aligned} \tag{A.9}$$

where $< \epsilon^*_{i,f} >$ is the average of the rates computed by `TIDES` for the shell S at two successive radii values, and t_i and t_f are the times corresponding to the shell radii r_i and r_f.

This equation gives the time it takes the N layers L to expand from an initial average radius r_i to a final average radius r_f, due to the energy input $< \epsilon^*_{i,f} >$, the latter being the average of the computed ϵ^*_i values at each of the two above-mentioned radii.

Finally, substituting t_{if} into equation (9) yields the time that has transpired since the start of asynchronous rotation.

REFERENCES

Adame, L., D'Alessio, P., Calvet, N. Cantó, J. 2011, RMxAC, 40, 263

Alexander, M.E. 1973, Ap&SS, 23, 459

Baruteau, C. et al. 2013 in Protostars and Planets VI, ed. H. Beuther et al. (AZ:UAP), 667

Berger, E., Soderberg, A. M., Chevalier, R. A., et al. 2009, ApJ, 699, 1850

Bodenheimer, P.H., Lin, D.N.C., & Mardling, R.A. 2001, ApJ, 548, 466

Dall'Osso, S. & Rossi, E.M. 2014, MNRAS, 443, 1057

Eggleton, P.P, Kiseleva, L.G., Hut, P. 1998, ApJ, 499, 853

Gu, Pin-Gao, Bodehnheimer, P.H., & Lin, D.N.C. 2004, ApJ, 608, 1076

Guenther, D.B., Demarque, P., Kim, Y.-C. & Pinsonneault, M.H. 1992, ApJ, 387, 372

Kamiński, T., Mason, E., Tylenda, R., Schmidt, M. 2015, A&A, 580, A34

Kochanek, C.S., Adams, S.M., & Belczynski, K. 2014, MNRAS, 443, 1319

Kulkarni, S. R., Ofek, E. O., Rau, A., et al. 2007, Natur, 447, 458

Leconte, J., Baraffe, I., Chabrier, G., Barman, T. & Levrard, B. 2009, A&A, 506, 385

Martini, P., Wagner, R. M., Tomaney A, et al. 1999, AJ, 118, 1034

Moreno, E., & Koenigsberger, G. 1999, RMxAA, 35, 157

Moreno, E., Koenigsberger, G., & Toledano, O. 2005, A&A, 437, 641

Moreno, E., Koenigsberger, G. & Harrington, D.M. 2011, A&A, 528, A48

Mould, J., Cohen, J., Graham, J. R., et al. 1990, ApJ, 353, L35

Munari, U., Henden, A., Kiyota, S., et al. 2002, A&A, 389, L51

Nakano, S. 2008, IAU Circ., 8972

Ogilvie, G.I. & Lesur, G. 2012, MNRAS, 422, 1975

Penev, K., Sasselov, D., Robinson, F., & Demarque, P. 2007, ApJ, 655, 1166

Penev, K., Barranco, J. & Sasselov, D. 2009, ApJ, 705, 285

Pérez de Tejada, H. 1999, ApJ, 525, 65

Press, W. H., Wiita, P.J. & Smarr, L.L. 1975, ApJ, 202, L135

Shakura, N. I., & Sunyaev, R. A. 1973, A&A, 24, 337

Soker, N. & Tylenda, R. 2003, ApJ, 582, L105

Stepień, K. 2011, A&A, 531A, 18S

Sutantyo, W. 1974, A&A, 35, 251

Tylenda, R. et al. 2011, A&A, 528, A114

G. Koenigsberger: Instituto de Ciencias Físicas, Universidad Nacional Autónoma de México, Ave. Universidad S/N, Col. Chamilpa, Cuernavaca, 62210, México (gloria@icf.unam.mx).

E. Moreno: (Instituto de Astronomía, Universidad Nacional Autónoma de México, Apdo. Postal 70-264, México, D.F., C.P. 04510, México (edmundo@astro.unam.mx).